1　*Article*

2 Travelling Surface Plasmons with Interference
3 Envelope and A Vision for Time Crystals

4　**Amir Djalalian-Assl** [1,*]

5　　[1] ORCID:0000-0002-7132-1085
6　　* Correspondence: amir.djalalian@gmail.com

7　**Abstract:** The influence of the film thickness and the substrate's refractive index on the surface mode
8　at the superstrate is an important study step that may help clearing some of the misunderstandings
9　surrounding their propagation mechanism. A single sub-wavelength slit perforating a thin metallic
10　film is among the simplest nanostructure capable of launching Surface Plasmon Polaritons on its
11　surrounding surface when excited by an incident field. Here, the impact of the substrate and the
12　film thickness on surface waves is investigated. When the thickness of the film is comparable to its
13　skin depth, SPP waves from the substrate penetrate the film and emerge from the superstrate,
14　creating a superposition of two SPP waves, that leads to a beat interference envelope with well-
15　defined loci which are the function of both the drive frequency and the dielectric constant of the
16　substrate/superstrate. As the film thickness is reduced to the SPP's penetration depth, surface waves
17　from optically denser dielectric/metal interface would dominate, leading to volume plasmons that
18　propagate inside the film at optical frequencies. Interference of periodic volume charge density with
19　the incident field over the film creates charge bundles that are periodic in space and time.

20　**Keywords:** surface plasmons; time crystal; thin film

21

22 1. Introduction

23　　In a most relevant report (to a certain extent) Wang *et. al.*[1] modelled a free standing optically
24　thin silver film in vacuum, where authors try to explain their findings in terms of long range SPPs,
25　SPP Wave Packets and Quasi Cylindrical Waves (QCW) … etc. Prior to that, Verhagen *et. al.* showed
26　that guided waves in a metal-dielectric-metal waveguide can penetrate the thin metallic cladding
27　hence shortening the wavelength of the SPPs at the silver/air interface [2].
28　　When the refractive index of the substrate differs from that of the superstrate, however, the
29　superposition of the two waves from both sides of the film leads to travelling SPP waves modulated
30　by a well define non-travelling interference envelope at metal/dielectric interfaces. For a sufficiently
31　thin metallic layer, SPPs formed at the metal/superstrate also interfere with those formed at the
32　metal/substrate within the metal leading to a non-travelling periodic electric polarization inside the
33　film. Note that this report is not concerned with the SPP eigenmodes [3-5], but rather it is an
34　investigation on surface wave interference under the forced vibration. The numerical results reported
35　here are exactly those included in chapter 10 of my thesis [6]. However, during the internal review,
36　pre- and post-examination period of my thesis, it was requested that I remove the notions of Lorentz
37　force and periodic transparency. This version of the report has those notions restored and used for
38　explaining the mechanism behind the plasmonic time-crystal and more.
39　　Let us start with the fundamental equations governing the surface plasmons polaritons (SPP)
40　stated here for convenience [7]:

$$41 \qquad k_{SPP} = \sqrt{\frac{\varepsilon_m \varepsilon_d}{\varepsilon_m + \varepsilon_d}} k \equiv k'_{SPP} + \mathrm{i}\, k''_{SPP} \qquad (1)$$

$$42 \qquad k_m \approx \sqrt{\frac{\varepsilon_m^2}{\varepsilon_m + \varepsilon_d}} k \equiv k'_m + \mathrm{i} k''_m \qquad (2)$$

43　　　There is also a very useful presentation by Rosa [8] that would help the reader to gain
44　background knowledge on SPPs. Not having access to the university resource, I could not cite the
45　references in that presentation. So, I hope citing Rosa's work would suffice for now.
46　　　Now, consider a metallic thin film with its surface set parallel to the *x*-*y* plane. Equation (1)
47　describes the complex wave vector for the SPP waves propagating at the metal/dielectric interface
48　along the *x*-*y* plane, whereas the wave vector for the SPP waves penetrating the metallic film in the
49　*z*-direction is given by equation (2). In both equations the real part of the wave vector represents
50　propagation constant, whereas the imaginary part defines the decay lengths, $1/k''_{SPP}$ and $1/k''_m$, over
51　which the SPP's amplitude decreases by 1/*e*. Note that in equation (2), the permittivity, ε_d,
52　corresponds to the dielectric material from which the field penetrates the film.
53　　　The short introduction above was aimed to highlight some of the key features of surface plasmon
54　polaritons relevant to this report. What will follow is a theoretical study on SPPs launched by a single
55　subwavelength aperture perforated in a silver thin film. Section 2.1 covers the influence of the film
56　thickness and the refractive index of the supporting substrate on the SPPs and in section 2.2 a
57　plasmonic time crystal is proposed.

58　**2. Results and Discussions**

59　*2.1 The Origin of Modulating Envelope in SPPs over Flat Metallic Films*

60　　　A 2D Finite Element Method (FEM) model of a 100 nm thick silver film perforated with a 50 nm
61　wide slit was simulated. Modelling time harmonics with FEM is particularly useful in examining the
62　steady-state response of the system under the continues excitation with an incident wave with a
63　single wavelength. The refractive index of the glass substrate supporting the film was initially set to
64　n_1 = 1.52 and the refractive index data for silver was taken from Palik [9]. The film was along the *x*
65　plane and was illuminated with a normally incident TM wave propagating in the +*z*-direction from
66　glass substrate. For convenience the air/silver interface is denoted by $z = z_0$. Figure 1(a) depicts the
67　distribution of the real part of surface charge densities, $\sigma(x,t) = |\sigma(x)| e^{i(k_{SPP}x - \omega_0 t)}$, at an arbitrary time
68　t_0, calculated at both the air/silver and glass/silver interfaces from the normal to the surface, i.e. the *z*-
69　component of the electric field. The amplitude, i.e. the envelope, of the surface charge density at the
70　air/silver interface was calculated using $|\sigma(x)| = \sqrt{\sigma(x,t)\sigma(x,t)^*}$ and is depicted in Figure 1(b). The
71　corresponding Fast Fourier Transforms (FFT), $f\left[\sigma(x,t_0)\right]$ and $f\left[|\sigma(x)|\right]$ were also calculated, see
72　Figure 1(c)-(d).
73
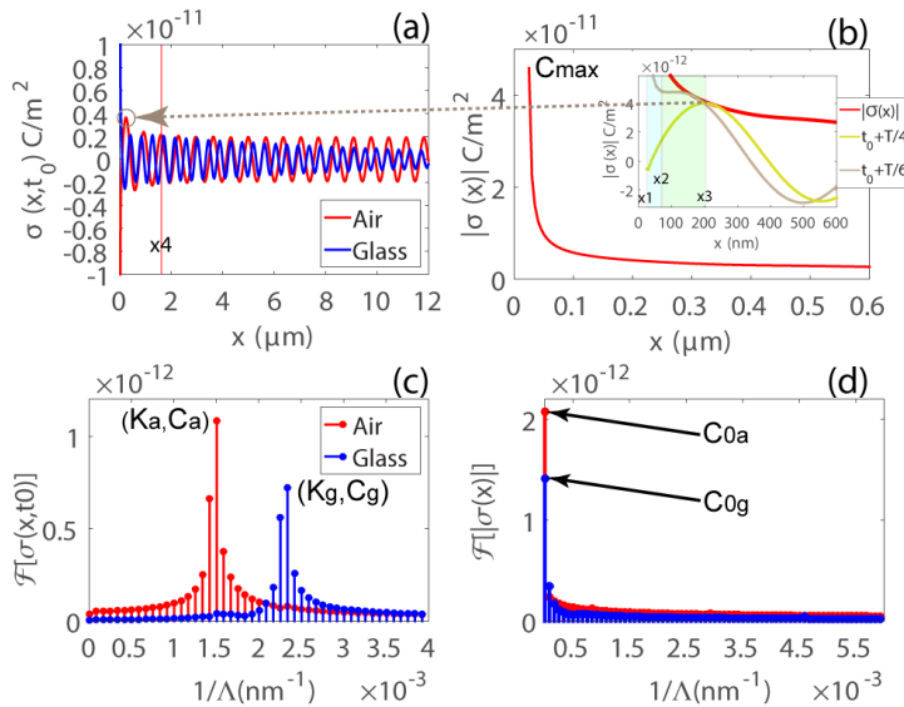
74

75   Figure 1: (a) Surface charge density, $\sigma(x, t_0)$, at an arbitrary time t_0, calculated at the air/silver and
76   glass/silver interfaces. (b) The envelope, $|\sigma(x)|$, at the air/silver interface. The corresponding FFT of
77   (c) the wave $f\left[\sigma\left(x, t_0\right)\right]$ and (d) the envelope $f\left[\left|\sigma\left(x\right)\right|\right]$ [6].

78   In Figure 1(b), the maximum accumulated charge density at the edge of the cavity, $x_1 = 25$ nm, is
79   labelled C_{max}. The decay length of the surface charge density, where the value of the C_{max} drop by $1/e$,
80   was found to be ~10 nm from the edge (or 35 nm from the center). At $\lambda_0 = 700$ nm, the decay length
81   of an SPP along the silver/air interface is ~67 μm [7]. Activities near the slit, therefore, may not be
82   considered as SPPs as they are highly localized. The inset of Figure 1(b), depict the $|\sigma(x)|$ and $\sigma(x,t)$
83   at $t = t_0 + T/6$ and $t_0 + T/4$. Here, T is the period and t_0 was set to a time when the surface charge density
84   was at its maximum, C_{max}, at x_1. The separation between the localized surface charges and the
85   appearance of the harmonic wave occurs at $t = t_0 + T/6$ and $x_2 \approx 75$ nm, i.e. 50 nm away from the edge.
86   In fact, the 10 nm decay length, closer to the $1/k_m'' \approx 25$ nm obtained from equation (2), indicates that
87   the surface charges in the vicinity of the slit are due to the cavity modes, penetrating the metal and
88   subsequently decaying rapidly. This agrees to previous works [10,11]. Furthermore, at $t = t_0 + T/4$ the
89   surface charge density at x_1 drops to 0 and the peak at $x_3 = 200$ nm resembles that of a harmonic wave.
90   The phase difference of 90° between the oscillations at x_1 and x_3, resembles that of a forced vibration
91   where the force leads the displacement by 90° under resonance conditions [12]. However, the
92   amplitude of the first peak at x_3 is $1.9 \times C_{0a}$, where C_{0a} is the DC component of $|\sigma(x)|$, hence the average
93   amplitude of the travelling SPP waves, see Figure 1(a) and (d). Note FFT of the envelope, $f\left[\left|\sigma\left(x\right)\right|\right]$
94   , in Figure 1(d), identifies the DC components (or the amplitudes of the SPP waves), C_{0a} and C_{0g} at
95   both interfaces.
96   By examining Figure 1(a) it was determined that the amplitude of the wave drops to C_{0a} at $x_4 \approx$
97    $w/2 + 2 \times \lambda_{SPP}$, i.e. 2 wavelengths away from the edge of the slit. Although the surface charge density
98   resembles that of a harmonic oscillation in the $x_3 \leq x \leq x_4$ range, its rapid decay and non-conformance
99   to the $1/k_{SPP}''$, suggests a kind of transient state. To evaluate the λ_{SPP}, FFT transform $f\left[\sigma\left(x, t_0\right)\right]$ was
100   calculated for both the silver/air and the silver/glass interfaces, Figure 1(c). The weighted average,
101   $K_{SPP} = \sum_{i=1}^{5} \left(K_{SPPi} C_{SPPi}\right) / C_{SPPi}$, that included the center mode and the four immediate neighboring
102   modes, i.e. two on each side of the maxima, provides a good estimate of SPP wavenumbers. The SPP

103 wavelengths were then calculated using $\lambda_{SPP} = 1/K_{SPP}$, where $K_{SPP} = \mathrm{Re}(k_{SPP})/2\pi$ is the wavenumber
104 obtained from FFT.

105   For the sake of brevity in notations, let the subscripts "a" and "g" be denoting the association of
106 physical quantities carried by the SPP waves at the superstrate (air) and substrate (glass and later
107 diamond) respectively. So, in summary, $\lambda_a = 1/K_a = 667$ nm and $\lambda_g = 1/K_g = 427$ nm are in agreement
108 with $\lambda_a = 682$ nm and $\lambda_g = 433$ nm obtained analytically using equation (1). Examining the $|\sigma(x)|$,
109 an additional spatial second harmonic were observed in the envelope at both interfaces. The second
110 harmonics in the envelope seems to be the result of superposition of two time-harmonic waves:

$$\sigma(x,t) = E_z e^{i(k_a x - \omega_0 t)} + E_{z?} e^{i(-k_a x - \omega_0 t + m\pi)} \qquad (3)$$

112 where m must be an even integer and $E_z \gg E_{z?}$. However, the origin of the second term in equation (3)
113 , $E_{z?}$, is unknown. The boundary conditions were set to eliminate all reflections, therefore, simulation
114 artefacts cannot account for such periodic perturbations, even more so that such second harmonics
115 do not manifest themselves over the surface of a Perfect Electric Conductor (PEC) that does not
116 support SPPs!

117   A possible scenario that may lead to oscillations at double the fundamental frequency in $|\sigma(x)|$,
118 is the normal-to-the-surface component of SPPs being modulated by the parallel-to-the-surface
119 component at the interface via a relationship that involved multiplication. SPPs are longitudinal
120 waves manifested as surface charge bundles, where charges in each bundle are held together by SPP's
121 E_z along the x-axis. Repelling/attracting Coulomb forces from each bundle to its neighboring charge
122 bundles of equal/opposite signs, is analogous to a chain of masses attached to one another by springs.
123 Given that the oscillation along the chain is being driven by $F \propto \sigma(x,t) E_x(z_0, t)$ from the aperture, it
124 is plausible to attribute the origin of the backward propagating term in equation (3) to
125 $F_x \propto e^{-i2(k_a x - \omega_0 t)}$, where the push/pull by F_x generates the backward propagating waves. Basically, the
126 force modulates the amplitude of the surface charge density wave over $T/2$, during which the SPP
127 has travelled a total distance of $\lambda_g/2$. Having noted that, the exact form of a partial differential
128 equation governing the forced vibration that leads to equation (3) as a solution is yet to be
129 determined.

130   Regardless, it was envisaged that by reducing the film thickness, it would be possible for surface
131 charge densities from the glass/silver interface manifest themselves at the air/silver interface, leading
132 to a superposition of the two waves:

$$\sigma(x) = \left[2e^{i\left(\frac{(k_a+k_g)x}{2}\right)} \cos\left(\frac{(k_a-k_g)x}{2}\right) \right] \qquad (4)$$

134 see Appendix A. This would modulate the charge densities along the x-direction, resulting in a series
135 of minima/maxima with fixed loci that are $1/K_{beat}$ apart, where $K_{beat} \equiv |K_a - K_g|$. Hence by controlling
136 the film thickness and the refractive index of the substrate, one could control the modulation strength
137 and frequency of the envelope. Keeping the superstrate and the substrate intact as before, two
138 additional simulations, with $h = \{50, 25\}$ nm, were carried out in order to investigate the influence of
139 the film thickness. Figure 2 depict the numerically calculated $f\left[\sigma(x,t_0)\right]$ and $f\left[|\sigma(x)|\right]$. Figure
140 2(a), (c) and (e) depicts $f\left[\sigma(x,t_0)\right]$ with $h = \{50, 25\}$ nm when the film is supported on a glass
141 substrate and with $h = 25$ nm on a diamond substrate respectively. In all cases, K_a was found to be at
142 the same position as it was for $h = 100$ nm. For $h = \{50, 25\}$ nm on a glass substrate, K_g was also found
143 to be at the exact location as it was for the 100 nm thick silver film. In the case of the diamond
144 substrate, $\lambda_g = 1/K_g = 230$ nm, was found to be close to the $\lambda_g = 246$ nm calculated using equation (1)
145 . In all cases, the appearance of an additional peak at the air/silver interface, positioned at K_g having
146 an amplitude $C_{\delta g} = C_g e^{-\frac{z}{\delta}}$, corresponded to the SPP waves that travel along the substrate/silver
147 interface penetrating the film and emerging at the air/silver interface. Presence of SPPs with
148 wavelength λ_g at air/silver interface is significant as it impacts the design criteria for plasmonic meta-

149   surfaces. FFT of the corresponding envelopes, $f\left[\left|\sigma(x)\right|\right]$, in Figure 2(b), (d) and (f), show the

150   anticipated modulating envelope with $K_{\text{beat}} \equiv |K_a - K_g|$.

151
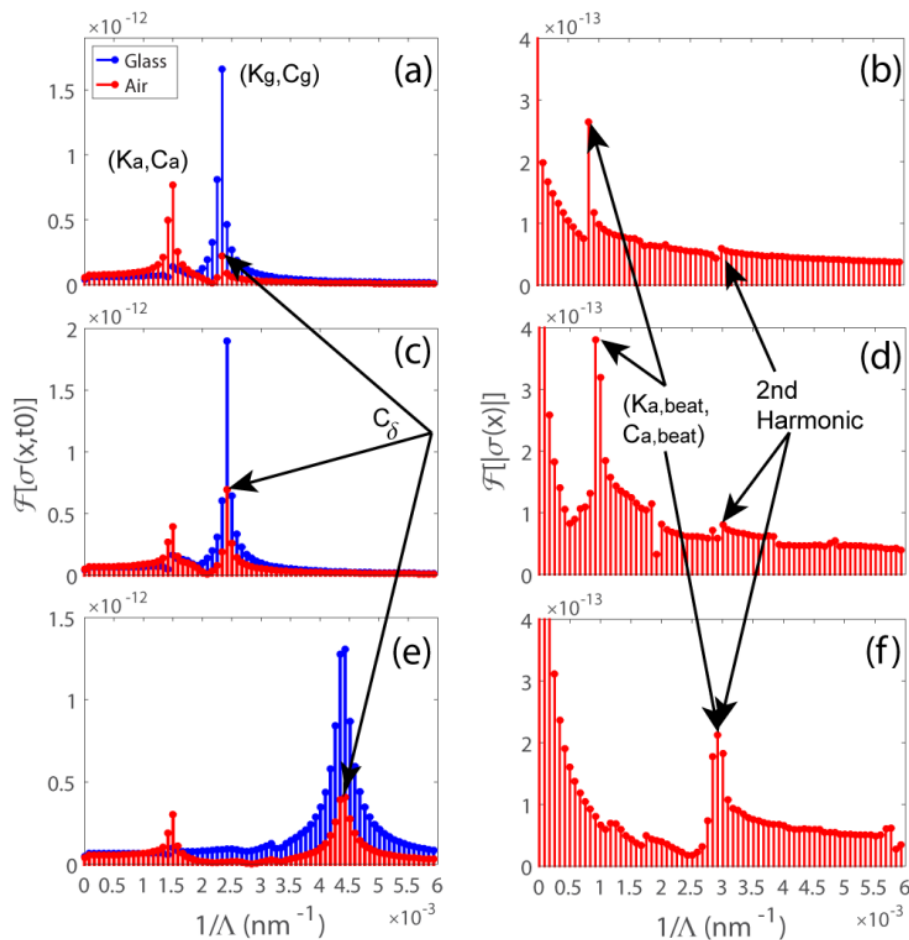
152

153   Figure 2: $f\left[\sigma(x,t_0)\right]$ and $f\left[\left|\sigma(x)\right|\right]$ calculated for (a)-(b) $h = 50$ nm on glass substrate, (c)-(d) $h =$

154   25 nm on glass substrate and (e)-(f) $h = 25$ nm on diamond substrate. Note that subscript 'g' is used to

155   label the substrate in general [6].

156   Note that in order to shift the K_{beat} to overlap with the second harmonics observed in the

157   envelope, the required value for the substrate's refractive index was found to be (see Appendix A)

158   $n_1 = 2.41$ at $\lambda_0 = 700$ nm that corresponds to diamond [13]. With the recent advances in nano-diamond

159   technology, use of diamond substrate is both feasible and practical [14]. Therefore, an additional

160   simulation was carried out with a 25 nm thick silver film supported on a diamond substrate.

161   Figure 3 depicts the modulating envelopes, $|\sigma(x)|$, calculated over the air/silver interface for

162   $h = \{100, 50, 25\}$ nm when the film is supported on a glass substrate and for $h = 25$ nm with a diamond

163   substrate. The aperture was normally illuminated with a Gaussian beam, $15 \times \lambda_0$ in waist, from the

164   substrate. The surface of a perfect electric conductor (PEC) that neither supports SPPs nor allows the

165   penetration of the fields, produced only a smooth line, see Figure 3-(line in black). Values for the PEC

166   line were calculated using $\varepsilon_0 E_z$ to retain the C/m² unit. The inset in Figure 3 shows the travelling

167   SPPs, $\sigma(x, t)$, that are modulated by the envelope $|\sigma(x)|$, calculated over the air/silver interface for

168   the case $h = 50$ nm when excited with a plane wave from the glass substrate. The presence of the

169   second harmonic and the beat interference in the envelope are marked.
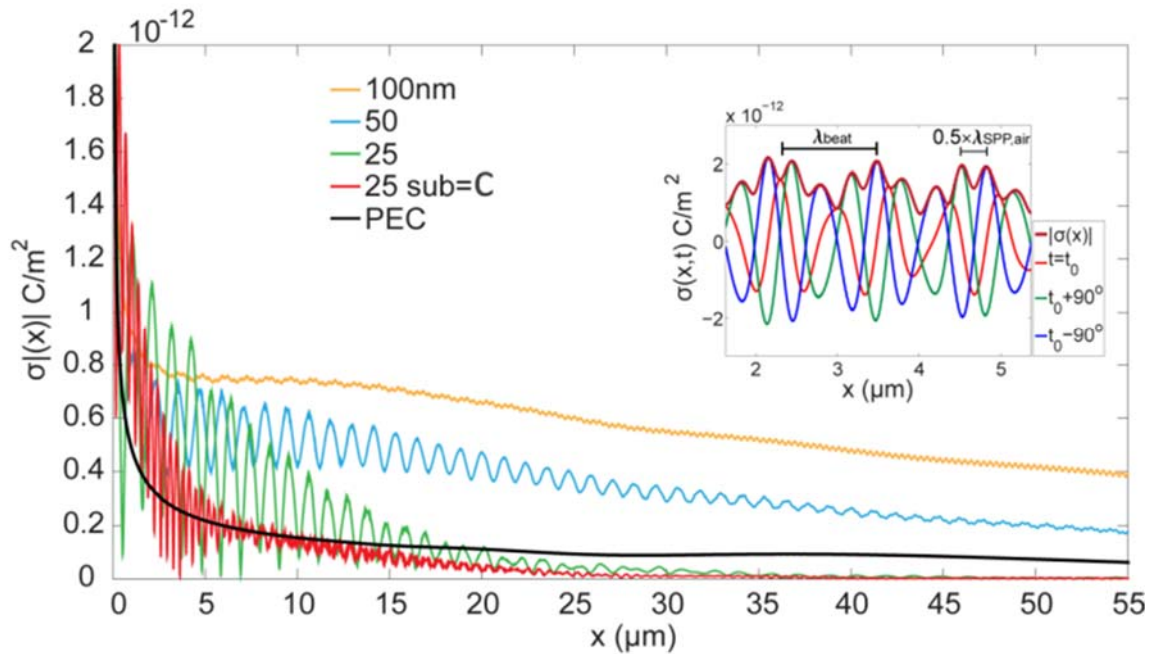
170

171   Figure 3: Surface charge densities, $|\sigma(x)|$, over the air/silver surface for h = {100, 50, 25} on glass
172   substrate, h = 25 nm on diamond substrate and for PEC [6].

173   A noticeable feature in Figure 3 is the relation between the SPP's decay length, $1/k_{SPP}''$, along the
174   air/silver interface and the strength (or the amplitude) of the interference envelope. Travelling SPP
175   waves along the air/silver interface may be described as the superposition of two waves according to
176   equation (A4) in Appendix A, where each component decay according to their respective decay
177   length $1/k_a''$ and $1/k_g''$. Analytical values for decay lengths were found to be {67, 17, 3.2) μm for the
178   air/silver, glass/silver and diamond/silver interfaces respectively. This explains the decay length of
179   the envelope clearly. For example, in the case of the 25 nm silver film supported on a diamond
180   substrate, the amplitude of the $C_{\delta g} e^{i(k_g x - \omega_0 t)}$ component drops to $1/e$ of its maximum at x = 3.2 μm,
181   beyond which the only component that continues to propagate is $C_{0a} e^{i(k_a x - \omega_0 t)}$ due to its longer decay
182   length of ~67 μm. And since the modulating envelope with K_{beat} requires the presence of both
183   components at the air/silver interface, the decay length of the envelope is dictated by the component
184   having the shortest of the two decay lengths, which in this example is 3.2 μm associated with the
185    $C_{\delta g} e^{i(k_g x - \omega_0 t)}$. Experimental measurements of such effects, however, may not be possible. Although
186   measurements carried out by Verhagen *et. al.* [2] *may* be valid, Wang *et. al.*[1] correctly pointed out
187   that positioning any probe such as an AFM tip, in the vicinity of the slit stablishes standing wave
188   oscillations between the tip and the slit, leading to a series of minima/maxima that convolve with
189   those of the interference envelope. FEM simulations has confirmed this.
190   The concept of plasmonic microzones [15,16] are not something new. What sets apart what I
191   have reported here is the formation of the periodic screening/transparency (i.e. the zone plate) by the
192   SPPs alone, and not during the fabrication. For the diamond substrate, diffraction patterns through a
193   25 nm silver film with single hole when excited with a normally incident beam (Gaussian in x) having
194   a waist of 2×λ_0, is shown in Figure 4(a). When the maximum intensity of the Gaussian beam falls
195   away from the centre of the slit (an arbitrary displacement of 680 nm in this case) the intensity of the
196   transmitted beam exhibits a curvature and a tilt towards the displacement, with the transmitted beam
197   being split in two, Figure 4(b). Such light-matter interaction is not observed in the transmitted beam
198   through a 25 nm silver film on a diamond substrate with no aperture, see Figure 4(c).
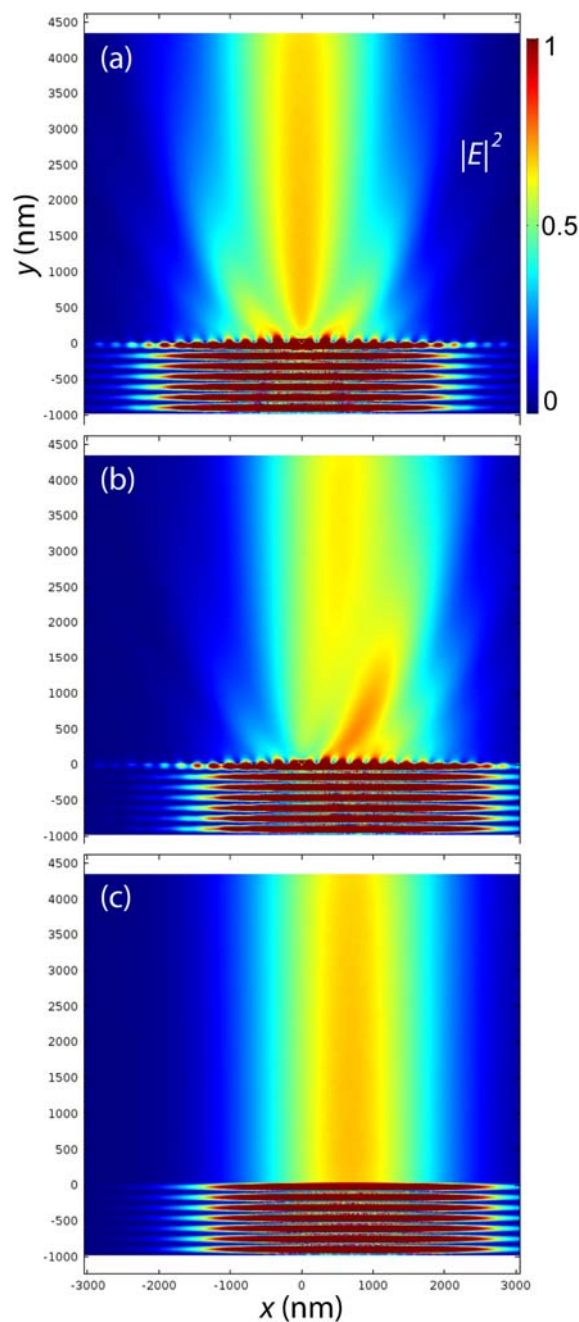
Figure 4: $|E|^2 \times 10 (\text{V/m})^2$ Diffraction patterns of a transmitted Gaussian beam through (a) 25 nm silver film perforated with a slit, supported on a diamond substrate. (b) same as (a) with the maximum intensity of the Gaussian beam displaced to $x = 680$ nm away from the centre of the slit. (c) In the absence of the slit [6].

2.2 Roadmap to Further Study and a Vision for Plasmonic Time Crystal

With diamond (or glass) substrate, when the film thinness is that of the skin depth, SPPs are no longer confined to the surface of the metal but rather penetrate the film from the substrate and superstrate and interfere with one another inside the film. However, (as it is the case here), due to the aperture dimensions and partially due to the $\varepsilon_m E_{zm} = \varepsilon_d E_{zd}$ [8], normal to the surface component of the electric field at the diamond/silver boundary is much stronger than those at the air/silver at $\lambda_0 = 700$ nm, hence $E_{zg} >> E_{za}$. Therefore, fields from the substrate dominate the film. Furthermore, the *x*-component of the SPP was found to be stronger than its *z*-components at $\lambda_0 = 700$ nm, i.e.

212 $E_{xg} \approx 2E_{zg}$ calculated using $E_{xg} = -i\sqrt{\dfrac{-\varepsilon_m}{\varepsilon_d}} E_{zg}$ [8], and in agreement with the numerical results.

213 Furthermore a trail of z-component of the electric field $\{\ldots 0 - 0 + 0 - 0 \ldots\}$ carries a trail of x-component

214 $\{\ldots - 0 + 0 - 0 + \ldots\}$ with "+", "0" and "-" denoting $+E_{x,z}$, 0 and $-E_{x,z}$ respectively. Note the 90° phase

215 difference between the x and the z-components. Naturally, the induced periodic polarization, travels

216 inside the film as the SPPs propagate over the surface. The x-component of the polarization,

217 $P_{xg} = \varepsilon_0 \chi_e E_{xg} e^{i(k_g x - \omega_0 t)}$, is of interest in the context of plasmonic time crystals as it signifies periodic

218 accumulation of conduction electrons along the x-axis, hence periodic screening/transparency within

219 the film that resembles that of a Fresnel zone plate.

220

221 With a flat metallic film that extends to infinity in the x-direction, it is not possible to apply the

222 Gauss's law to calculate the charges due to SPP fields. Therefore, I have provided an alternative

223 approach to calculate the induced periodic charge density due to propagating E_{zg}:

224
$$\Delta \rho_x(k_g, \omega_0) = -\frac{\omega_0}{c} \varepsilon_0 \varepsilon_m^{''} \left[\frac{\varepsilon_d + \varepsilon_m}{\sqrt{\varepsilon_m + \varepsilon_d}}\right] E_{zg} e^{i(k_g x - \omega_0 t)} \qquad (5)$$

225 see Appendix B. And in terms of number of electrons being displaced:

226
$$\Delta N(k_g, \omega_0) = \frac{\Delta \rho_x}{e^{-}} = -\frac{\omega_0}{ce^{-}} \varepsilon_0 \varepsilon_m^{''} \left[\frac{\varepsilon_m + \varepsilon_d}{\sqrt{\varepsilon_m + \varepsilon_d}}\right] E_{zg} e^{i(k_g x - \omega_0 t)} \qquad (6)$$

227 Equation (6) reveals the total number of charges being displaced per SPP field. Given that the

228 fermi energy level for metals is given by $\mathcal{E}_F = \dfrac{h^2}{8m}\left(\dfrac{3N}{\pi}\right)^{2/3}$ [17], one must set $N = N_0 + \Delta N$, where N_0

229 is the number of electrons per unit volume when unperturbed.

230
$$\mathcal{E}_F(k_g, \omega_0) = \frac{3^{2/3} h^2}{8m\pi^{2/3}}(N_0 + \Delta N)^{2/3} \qquad (7)$$

231

232 Consequently, $\Delta \rho_x$, ΔN and $\mathcal{E}_F$ become a function (k_g, ω_0) due to $E_{zg} e^{i(k_g x - \omega_0 t)}$, which may lead to

233 many interesting effects, such as periodic refractive index, fermi levels, local work functions, density

234 of states, eigen energies inside film, which will be a topic of another report. Nevertheless, in the

235 absence of any incident field over the film, for example when the SPPs are launched by a dipole near

236 the surface [18], the propagation of surface waves, and all physical quantities they carry, is

237 unperturbed. However, in the presence of an incident field normal to the surface, the superposition

238 of the fields inside the film is given by $E = E_{xi} e^{i(k_i z - \omega_0 t)} + E_{xg} e^{i(k_g x - \omega_0 t)}$ which create disturbance on the

239 periodic charges densities. It is intuitive that loci polarized by $+E_{xg}$ be transparent to $+E_{xi}$, and vice

240 versa. Now, consider an arbitrary time $t = t_0$, when the maximum of the incident electric field falls

241 over the film. This is depicted by the following notation:

242
$$\frac{E_{xg}(x, t_0): +, 0, -, 0, +}{E_{xi}(t_0): +, +, +, +, +} \Rightarrow +, +, 0, +, + \qquad (8)$$

243 This scenario is shown in Figure 5 with the periodic arrangement of "0"s when the maximum of

244 the field falls over the film. Also note the strong periodic field under the film, inside the glass and

245 diamond substrates! At $t = t_0 + T/2$, hence 180° phase, both E_{xg} and E_i change sings. This will lead to:

246
$$\frac{E_{xg}(x, t_0 + T/2): -, 0, +, 0, -}{E_{xi}(t_0 + T/2): -, -, -, -, -} \Rightarrow -, -, 0, -, - \qquad (9)$$

247 with "0" remained intact in space as it was in the case of equation (8).   This scenario is also
248 confirmed by numerical results.

249

250 *It is intuitive to think of the periodic "0"s as loci where conduction electrons are trapped. If this hypothesis*
251 *is validated by experiment, it would open doors to study new phenomena. Each "0" may be viewed as a super-*
252 *atom with oversaturated electronic orbitals, elevated fermi level, lowered work function and many more effects*
253 *when considered in periodic settings which I have highlighted in the conclusion.*

254

255 Back to causality, at the first glance it seems it is a simple matter of superposition of two
256 orthogonally propagating EM waves with the *x*-component of the two fields summed up inside the
257 film. However, a close look at the numerical results revealed that when E_{xi} drops to 0, (e.g. at
258 $t = t_0+T/4$), polarization inside the film experiences the effect of $E_{xi}(t_0)$. This 90° phase difference
259 between applied filed and the reaction is attributed to the charge bundles experiencing the Lorentz
260 force $F_{xg} = J_{zg}(B_{yg} + B_{yi})$. Furthermore, since B_{yi} is 0 at $t = t_0+T/4$, the restoration of periodic potential
261 is resumed at $t = t_0+T/4$ but completed at $t = t_0+T/2$ when $-E_{xi}$ falls over the film. The whole
262 creation/anhelation of $P_x = \varepsilon_0 \chi_e E_x$ is a sinusoidal process in time. Numerical results also revealed
263 that E_{zg} not being affected by the *incident* field. Therefore, the restoration process is attributed to the
264 E_{zg}. Since this creation/anhelation is periodic both in time and space with periodicities $T/2$ and λ_g,
265 hence oscillating at frequency other than that of the drive, (although not an expert in the topic), I
266 believe it qualifies as a time crystal [19,20]. As for the breaking time symmetry, I need access to certain
267 resources only academics enjoy, but as an alumnus, this is not possible at this stage. However, I must
268 remind the readers that the *x*-component of the SPP's electric field (as I understand) must always lag
269 its *z*-components by 90° at *resonance*, a condition satisfied for SPPs launched by an aperture at any
270 frequency.

271
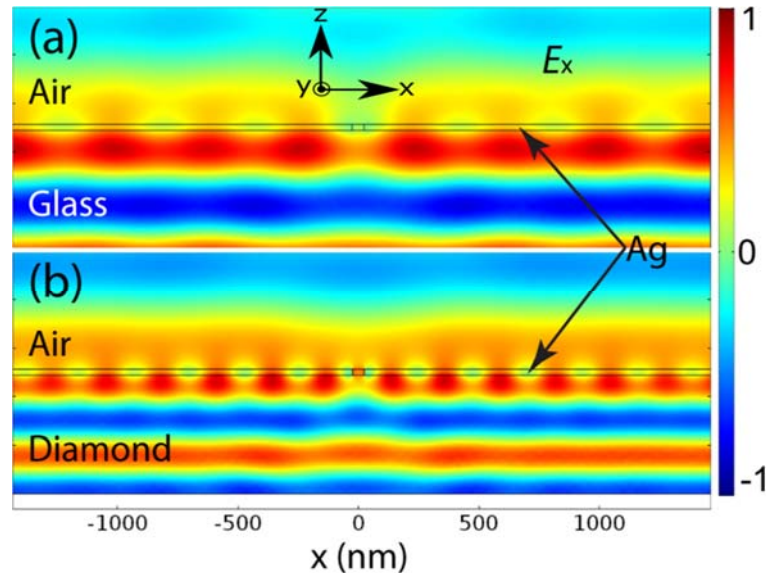
272

273 Figure 5: Snapshot of electric field E_x passing through a periodic charge screen (with periodicity $1/K_g$)
274 formed inside the 25 nm thick silver film for (a) glass and (b) diamond substrates. Note that E_x was
275 calculated at an arbitrary time with the maximum of its amplitude falling over the silver film [6].

276 The term *crystal* also implies that one should be able to define both the Hamiltonian to determine
277 the eigen-energies and the Schrödinger equation to explain the De Broglie's matter waves [21,22] for
278 that system. The potentials *V*, experienced by electrons in a time crystal and consequently, wave
279 functions ψ and eigen-energies ξ, must naturally be time-dependent:

280 $$\xi_j(t)\psi_j(\mathbf{R}_j,t) = \hat{H}(t)\psi_j(\mathbf{R}_j,t) \qquad (10)$$

281
$$i\hbar \frac{\partial \psi_j (\mathbf{R}_j, t)}{\partial t} = \hat{H}(t) \psi_j (\mathbf{R}_j, t) \qquad (11)$$

282

283   Considering the original Hamiltonian, $\hat{H}$, for the many-electrons [23]:

284

285
$$\hat{H} = \sum_j \left[-\frac{\hbar^2}{2m} \nabla_j^2 + V(\mathbf{R}_j) \right] + \frac{1}{2} \sum_{\substack{j,k \\ j \neq k}} \frac{e^2}{4\pi\varepsilon |\mathbf{R}_j - \mathbf{R}_k|} \qquad (12)$$

286   Time variations of kinetic energy term in equation (12) is taken care of by the time-dependent
287   wave function $\psi_j (\mathbf{R}_j, t)$, however, one must introduce the notion of time into equation (12) and
288   rewrite it as:

289
$$\hat{H}(t) = \sum_j \left[-\frac{\hbar^2}{2m} \nabla_j^2 + V(\mathbf{R}_j(t)) \right] + \frac{1}{2} \sum_{\substack{j,k \\ j \neq k}} \frac{e^2}{4\pi\varepsilon |\mathbf{R}_j(t) - \mathbf{R}_k(t)|} \qquad (13)$$

290

291   where $V(\mathbf{R}_j(t)) = V_{ext}(\mathbf{R}_j(t)) + V_t(\mathbf{R}_j(t), t)$, V_{ext} is the potential due to the positive ions, $V_t \propto e^{i(k_g x - \omega_0 t)}$ is
292   the time-dependent potential due to the creation/anhelation of charge bundles and $\mathbf{R}_j$ is the position
293   vector of the jth electron. Note that by making $\mathbf{R}_{j,k}$ time-dependent, $j \neq k$ is taken care of, however, V_t
294   has both time and spatial dependence (other than that of positive ions). Time-dependent Hamiltonian
295   in Equation (13) implies that the computation must trace the position of each electron, $\mathbf{R}_j$ with
296   respect to t and the changes in potential with respect to t and $\mathbf{R}_j$. The Hartree approximations [23]
297   are also based on time-independent electron-electron interactions, so it must be remedied accordingly
298   for time crystals. An interesting article by Linde [24] may prove to be useful to investigate possible
299   changes to the effective mass and conductivity in an applied field but that also needs to be modified.
300   With the advent of High Performance Computing (HPC) ab initio modelling and simulations of
301   matters where the constituting components are atoms and electrons are becoming more accessible.
302   An article by Borysov *et. al.* [25] provides a background on the existing infrastructure for numerically
303   modelling and investigating structures at atomic levels using the Density Functional Theory (DFT)
304   calculations, which may prove to be a platform of choice to study time crystals.

305   **5. Conclusions**

306   In conclusion, it was shown that for a sufficiently thin silver film sandwiched between two
307   different dielectrics, the mixing of the two SPPs (formed at the substrate and the superstrate) produce
308   an interference envelope that modulates the travelling SPPs. For film thicknesses equivalent to the
309   SPP's penetration depth, surface waves from optically denser dielectric/metal interface would
310   dominate, leading to volume plasmons that propagate inside the film at optical frequencies.
311   Interference of such volume charges with the incident field over the span of the film creates charge
312   bundles that are periodic in space and time. Although many questions remained unanswered in this
313   report, the future work will focus on them. I would hypothesize that the presence of charge bundles
314   inside the film may imply changes to the electronic density of states, electron-electron collision (hence
315   the mean free path), electron-lattice interaction (hence the electron's effective mass) and consequently
316   conductivity, due to the presence of an additional periodic potential that may compete or superpose
317   with that of the positive ions. It is intuitive to think of the periodic "0"s as loci where electrons
318   trapped. If this hypothesis is validated by experiment, it would open doors to study new phenomena.
319   Each "0" may be viewed as super-atom with oversaturated electronic orbitals, elevated fermi level,
320   lowered work function and many more effects when considered in periodic settings which are
321   analogous to that of a superlattice in semiconductors[23].

322

323   **Funding sources:** There were no founding sponsors supporting this work.

324

325   **Conflicts of Interest:** The authors declare no conflict of interest. Apart from the named author, no
326   other person or entity had any role in the inception or the design of the study; in the collection,
327   analysis, or interpretation of data; in the writing of the manuscript, and in the decision to publish the
328   results.

329   **Appendix A – Superposition**

330   To explain the overlap between the beat modulation and the second harmonics in the envelope
331   when $n_1 = 2.41$ at $\lambda_0 = 700$ nm, consider the superposition of two waves having equal amplitudes
332   propagating along the x-axis i.e. $\Psi(x,t) = e^{i(k_1 x - \omega_1 t)} + e^{i(k_2 x - \omega_2 t)}$, which can be written as:

$$\Psi(x,t) = 2e^{i\left(\frac{(k_1+k_2)x}{2} - \frac{(\omega_1+\omega_2)t}{2}\right)} \cos\left(\frac{(k_1-k_2)x}{2}\right)\cos\left(\frac{(\omega_1-\omega_2)t}{2}\right) \qquad \text{(A1)}$$

334   Here it is assumed both waves start in phase. This form of the equation is of interest since it
335   separates the terms related to the coherent length, $4\pi/(k_1 + k_2)$, and the coherent time, $4\pi/(\omega_1 + \omega_2)$
336   of the superposed travelling wave. Furthermore, the last two cosine terms indicate that the combined
337   travelling wave is modulated by two envelopes having nodes (or anti-nodes) separated by
338    $\left|\cos\left(\frac{(k_1-k_2)x}{2}\right)\right|$ in space and $\left|\cos\left(\frac{(\omega_1-\omega_2)t}{2}\right)\right|$ in time. In other words the beat frequencies in space
339   and time are $|k_1 - k_2|$ and $|\omega_1 - \omega_2|$ respectively, therefore the coherent lengths (for a lack of a better
340   word) of the envelopes in space   and time can be calculated as $2\pi/(k_1 - k_2)$ and $2\pi/(\omega_1 - \omega_2)$
341   respectively. Necessary conditions to eliminate undesirable jitters in space and time envelopes are:

$$\left[2\pi/(k_1 - k_2)\right] = \left[4\pi/(k_1 + k_2)\right] \qquad \text{(A2)}$$

343   AND

$$\left[2\pi/(\omega_1 - \omega_2)\right] = \left[4\pi/(\omega_1 + \omega_2)\right] \qquad \text{(A3)}$$

345   In the case of two superposed SPP waves at the air/silver interface, the superposition may be
346   simplified to:

$$\sigma(x,t) = e^{-i\omega_0 t}\left[C_a e^{i(k_a x)} + C_{\delta g} e^{i(k_g x)} \right] \qquad \text{(A4)}$$

348   Furthermore, in the case of 25 nm silver film $C_{\delta g} \approx C_a$, see Figure 2(c) and (e). Under such
349   conditions, equation (A4) may be written for the spatial terms as:

$$\sigma(x) = \left[2e^{i\left(\frac{(k_a+k_g)x}{2}\right)} \cos\left(\frac{(k_a-k_g)x}{2}\right) \right] \qquad \text{(A5)}$$

351   Equation(A5), which is the special case of equation(A1), shows the coherent length of the
352   combined travelling SPP waves to be $4\pi/(k_a + k_g)$ with the beat modulation occurring according to
353    $2\pi/|k_a - k_g|$. A necessary condition to overlap the coherent length and the beat modulation with the
354   second harmonics in the envelope is then:

$$1/2k_a = 2\pi/|(k_a - k_g)| = 4\pi/(k_a + k_g) \qquad \text{(A6)}$$

356   In this report, numerical values for wavenumbers obtained from FFT showed
357   $1/2K_a \approx 1/\left|K_a - K_g\right| \approx 2/\left|K_a + K_g\right|$ at $\lambda_0 = 700$ nm when $n_1 = 2.41$. Clearly in the case of a glass
358   substrate with $n_1 = 1.52$, $1/2K_a \neq 1/\left|K_a - K_g\right| \neq 2/\left|K_a + K_g\right|$ at $\lambda_0 = 700$ nm.

359   The appendix is an optional section that can contain details and data supplemental to the main
360   text. For example, explanations of experimental details that would disrupt the flow of the main text,
361   but nonetheless remain crucial to understanding and reproducing the research shown; figures of
362   replicates for experiments of which representative data is shown in the main text can be added here
363   if brief, or as Supplementary data. Mathematical proofs of results not central to the paper can be
364   added as an appendix.

365   **Appendix B - Lorentz Force and Induce Charges Inside the Film**

366   Let the magnetic flux density and the electric field carried by SPPs be denoted by:
367

368
$$\mathbf{B}_m = \left(0, B_y, 0\right) e^{i(k_x x + k_z z - \omega_0 t)} \qquad \text{(B1)}$$

369
$$\mathbf{E}_m = \left(E_x, 0, E_z\right) e^{i(k_x x + k_z z - \omega_0 t)} \qquad \text{(B2)}$$

370   For simplicity, ignoring the exponent terms, we are interested in $F_x = J_z B_y$ where $J_z = \sigma_e E_z$.
371   Given that $\mathbf{B}_m = \dfrac{\nabla \times \mathbf{E}_m}{j\omega_0}$

372   and

373
$$\nabla \times \mathbf{E}_m = \begin{pmatrix} \partial_x \\ \partial_y \\ \partial_z \end{pmatrix} \times \begin{pmatrix} E_x \\ 0 \\ E_z \end{pmatrix} = \begin{pmatrix} \partial_y E_z \\ -\partial_x E_z + \partial_z E_x \\ \partial_y E_x \end{pmatrix} \quad \text{(B3)}$$

374   In 2D:

375
$$\nabla \times \mathbf{E}_m = \begin{pmatrix} 0 \\ -ik_x E_z + ik_z E_x \\ 0 \end{pmatrix} \qquad \text{(B4)}$$

376   One can write $B_y = \dfrac{k_x E_z - k_z E_x}{\omega_0}$. The Lorentz force distribution along the x-axis is then

377   $F_x = J_z B_y = \sigma_m E_z \dfrac{k_x E_z - k_z E_x}{\omega_0}$. This can be further reduced by $E_x = -i\sqrt{\dfrac{-\varepsilon_m}{\varepsilon_d}} E_z$ to:

378
$$F_x = \frac{\sigma_m}{\omega_0}\left[k_x + k_z \left(i\sqrt{\frac{-\varepsilon_m}{\varepsilon_d}} \right) \right] E_z^2 \qquad \text{(B5)}$$

379   Using equations (1)-(2) and replacing $\sigma_m = \omega_0 \varepsilon_0 \varepsilon''_m$ [26], the Lorentz force becomes:

380
$$F_x = \frac{\omega_0 \varepsilon_0 \varepsilon''_m}{c}\left[\frac{\sqrt{\varepsilon_m \varepsilon_d} + i\varepsilon_m\sqrt{\dfrac{-\varepsilon_m}{\varepsilon_d}}}{\sqrt{\varepsilon_m + \varepsilon_d}} \right] E_z^2 \qquad \text{(B6)}$$

381
382   The volume charge profile along the *x*-direction due to only the Lorentz force may be calculated
383   as $\Delta\rho_x = F_x / E_x$ where $E_x = -i\sqrt{\dfrac{-\varepsilon_m}{\varepsilon_d}} E_z$, therefore:

384
$$\Delta\rho_x = -\frac{\omega_0}{c}\varepsilon_0\varepsilon_m^{"}\left[\frac{\varepsilon_d+\varepsilon_m}{\sqrt{\varepsilon_m+\varepsilon_d}}\right]E_z \quad (B7)$$

385   And in terms of number of free electrons:

386
$$\Delta N = \frac{\Delta\rho_x}{e^-} = -\frac{\omega_0}{ce^-}\varepsilon_0\varepsilon_m^{"}\left[\frac{\varepsilon_d+\varepsilon_m}{\sqrt{\varepsilon_m+\varepsilon_d}}\right]E_z \qquad (B8)$$

387   **References**

388 1. Wang, L.M.; Zhang, L.X.; Seideman, T.; Petek, H. Dynamics of coupled plasmon polariton wave packets excited
389   at a subwavelength slit in optically thin metal films. *Phys. Rev. B* **2012**, *86*.
390 2. Verhagen, E.; Dionne, J.A.; Kuipers, L.; Atwater, H.A.; Polman, A. Near-field visualization of strongly confined
391   surface plasmon polaritons in metal-insulator-metal waveguides. *Nano Lett.* **2008**, *8*, 2925-2929.
392 3. Davis, T.J. Surface plasmon modes in multi-layer thin-films. *Opt. Commun.* **2009**, *282*, 135-140.
393 4. Berini, P. Long-range surface plasmon polaritons. *Advances in Optics and Photonics* **2009**, *1*, 484-588.
394 5. Ortuno, R.; Garcia-Meca, C.; Rodriguez-Fortuno, F.J.; Marti, J.; Martinez, A. Role of surface plasmon polaritons on
395   optical transmission through double layer metallic hole arrays. *Phys. Rev. B* **2009**, *79*.
396 6. Djalalian-Assl, A. Optical nano-antennas. PhD, The University of Melbourne, Melbourne, 2015.
397 7. Novotny, L.; Hecht, B. *Principles of nano-optics*. Cambridge, U.K. : Cambridge University Press, 2006.: 2006.
398 8. Rosa, A.L. Lectures 9: Surface plasmon polaritons. http://web.pdx.edu/~larosaa/Applied_Optics_464-
399   564/Lecture_Notes_Posted/2010_Lecture-
400   7_SURFACE%20PLASMON%20POLARITONS%20AT%20%20METALINSULATOR%20INTERFACES/Lectu
401   re_on_the_Web_SURFACE-PLASMONS-POLARITONS.pdf
402 9. Palik, E.D. *Handbook of optical constants of solids*. Academic Press: San Diego, 1985; p 350.
403 10. Dai, W.; Soukoulis, C.M. Theoretical analysis of the surface wave along a metal-dielectric interface. *Phys. Rev. B*
404   **2009**, *80*, 155407.
405 11. Nikitin, A.Y.; Garcia-Vidal, F.J.; Martin-Moreno, L. Surface electromagnetic field radiated by a subwavelength
406   hole in a metal film. *Phys. Rev. Lett.* **2010**, *105*.
407 12. Main, I.G. *Vibrations and waves in physics*. Cambridge University Press: 1987.
408 13. Phillip, H.R.; Taft, E.A. Kramers-kronig analysis of reflectance data for diamond. *Physical Review a-General Physics*
409   **1964**, *136*, 1445-&.
410 14. Fairchild, B.A.; Olivero, P.; Rubanov, S.; Greentree, A.D.; Waldermann, F.; Taylor, R.A.; Walmsley, I.; Smith, J.M.;
411   Huntington, S.; Gibson, B.C., *et al.* Fabrication of ultrathin single-crystal diamond membranes. *Adv. Mater.* **2008**,
412   *20*, 4793-4798.
413 15. Fu, Y.; Zhou, W.; Lim, L.E.N.; Du, C.L.; Luo, X.G. Plasmonic microzone plate: Superfocusing at visible regime.
414   *Appl. Phys. Lett.* **2007**, *91*.
415 16. Chen, W.B.; Abeysinghe, D.C.; Nelson, R.L.; Zhan, Q.W. Plasmonic lens made of multiple concentric metallic
416   rings under radially polarized illumination. *Nano Lett.* **2009**, *9*, 4320-4325.
417 17. Eisberg, R.M.; Resnick, R. *Quantum physics of atoms, molecules, solids, nuclei, and particles*. 2nd ed.; Wiley: New York,
418   1985.
419 18. Djalalian-Assl, A. Dipole emission to surface plasmon-coupled enhanced transmission in diamond substrates
420   with nitrogen vacancy center- near the surface. *Photonics* **2017**, *4*, 10.
421 19. Wilczek, F. Quantum time crystals. *Phys. Rev. Lett.* **2012**, *109*, 5.
422 20. Shapere, A.; Wilczek, F. Classical time crystals. *Phys. Rev. Lett.* **2012**, *109*, 4.
423 21. Ashcroft, N.W.; Mermin, N.D. *Solid state physics*. Holt: New York,, 1976; p xxi, 826 p.
424 22. Blu¨mel, R. *Advanced quantum mechanics the classical-quantum connection*. Jones and Bartlett Publishers: Sudbury,
425   Mass., 2011; p xii, 425 p.
426 23. Davies, J.H. *The physics of low-dimensional semiconductors : An introduction*. Cambridge University Press:
427   Cambridge, U.K. ; New York, NY, USA, 1998; p xviii, 438 p.
428 24. Linde, J.O. The effective mass of the conduction electrons in metals and the theory of superconductivity. *Physics*
429   *Letters* **1964**, *11*, 199-201.
430 25. Borysov, S.S.; Geilhufe, R.M.; Balatsky, A.V. Organic materials database: An open-access online database for data
431   mining. *Plos One* **2017**, *12*, 14.

432 26.   Lorrain, P.; Corson, D.R.; Lorrain, F. *Electromagnetic fields and waves : Including electric circuits*. Freeman: New York,
433   1988.
434